The NA44 Aerogel Cherenkov Trigger

Hubert van Hecke[1] and Douglas E. Fields[1]

Abstract

In this note we attempted to collect in one place all the information relating to the Aerogel counter.

[1] Los Alamos National Laboratory, Los Alamos, NM 87545, USA.

1 Introduction

The original design for enhancing the the event rate for kaons over pions in the NA44 spectrometer involved rejecting events at the trigger level which had a signal above threshold in the C1 detector. This would reject all events that had one or more pions in that detector. This works well for low multiplicity events where the number of pions expected in an event containing kaons is low. For lead beams however, the pion multiplicity was expected (and measured) to be sufficiently high so that nearly all events of interest contained at least one pion. Rejecting events containing pions would then reject nearly all kaon events as well.

In order to enhance one and two kaon events without rejecting events containing pions, we proposed and subsequently built an aerogel differential cherenkov detector. The basic idea of this detector was to count the number of kaons in an event (ignoring pions) in a manner fast enough to provide a trigger for event determination.

In this design, pions and kaons traversing an aerogel radiator produce cherenkov light at an angle to their path which depends upon the particle velocity. Since, in our spectrometer, all particles have the same momentum within 20%, pions and kaons have different and specific velocities and therefore produce cherenkov light at specific angles. This light can then be focussed into a ring whose diameter is proportional to the emission angle, and thus the particle type. Pions produce a ring of light with a larger radius than the ring produced by kaons. We then mask the larger (pion) ring and thus ignore pions. Photons in the smaller (kaon) ring are "counted", determining the number of kaons present.

This basic idea is, of course, complicated by many intricacies of cherenkov light production, light collection optics and other physics and technical considerations. In order to study these issues, a Monte Carlo simulator of the detector was written. This note is intended as a guide to these issues based upon results of the Monte Carlo, direct measurements of optical properties, analysis of results of prototype detectors and finally, the analysis of the 1994 lead beam data.

2 Definition of the task

The task of this detector is to provide a clean and efficient one- and two-kaon trigger in the NA44 Pb beam environment. Clean means: for every 1000 events which contain n pions + m<2 kaons it will give a false trigger less than ten times. Efficient means: for every 100 events which contain n pions + n$\geq$2 kaons, it will give a valid trigger at least 80 times. The figures of merit are then an 80% efficient two or more kaon trigger with a cleanliness of 1%.

This is a difficult goal to attain. Since there are many factors which play into the success or failure, they will be broken down here to the extent that they can be seperated.

3 Cherenkov light production

Cherenkov light is emitted in a medium when the velocity of a charged particle exceeds the velocity of light in that medium, which is c/n, where n is the index of refraction.

The light is emitted at a characteristic angle, θ given by

$$cos\theta = \frac{1}{\beta n} \tag{1}$$

where n is the index of refraction for the material and β is the velocity of the charged particle.

The number of photons emitted per unit length and per unit wavelength is given by [1]:

$$\frac{dN}{dxd\lambda} = 2\pi\alpha\frac{1}{\lambda^2}\Big(1 - \frac{1}{\beta^2 n^2}\Big) \tag{2}$$

where α is the fine structure constant and n can be dependent upon the wavelength, λ. If the variation of $n(\lambda)$ is small over the region of interest λ_1 to λ_2, then we can integrate this equation to get:

$$\frac{dN}{dx} = 2\pi\alpha sin^2\theta\Big(\frac{1}{\lambda_1} - \frac{1}{\lambda_2}\Big) \tag{3}$$

From this, we note that the initial wavelength distribution of cherenkov light scales as λ^{-2}, and thus is dominated by short wavelengths.

4 Aerogel

4.1 Index of refraction

Aerogel has attracted much interest in its use as a Cherenkov radiator for one reason - it has an index of refraction that is smaller than nearly all liquids and solids (only liquid helium is close), but larger than gasses at atmospheric pressure. In fact, in order to get close to the index of refraction we would like, $n = 1.02$, one would need gas pressures of the order of ten to twenty atmospheres. This would introduce a problem of thick windows - not to mention the safety aspects. Aerogel can be produced in a fairly wide range of indeces of refraction, from 1.004 to 1.060.

The particle species which we want to separate and identify, and their typical momentum range, generally determine the index of refraction of the radiator. For example, assume again that we want to identify kaons and pions. For separability, require that the kaon cherenkov ring diameter be 3/4 of the pion ring diameter. Using equation 1, we can write this separability requirement can as follows:

$\frac{\arccos(1/(\beta_K n))}{\arccos(1/(\beta_\pi n))} = \frac{3}{4}$

If we assume $\beta_\pi \approx 1.0$, we can solve for the momentum for a given n. Some typical values are listed in table 1:

radiator	n	θ_c	p (Gev/c)
glass	1.5	48.0°	0.7
liquid	1.1	25.0°	1.7
aerogel	1.02	11.0°	3.7
freon (gas, 1 atm)	1.001	2.6°	17.0
helium (1 atm)	1.00035	0.5°	90.0

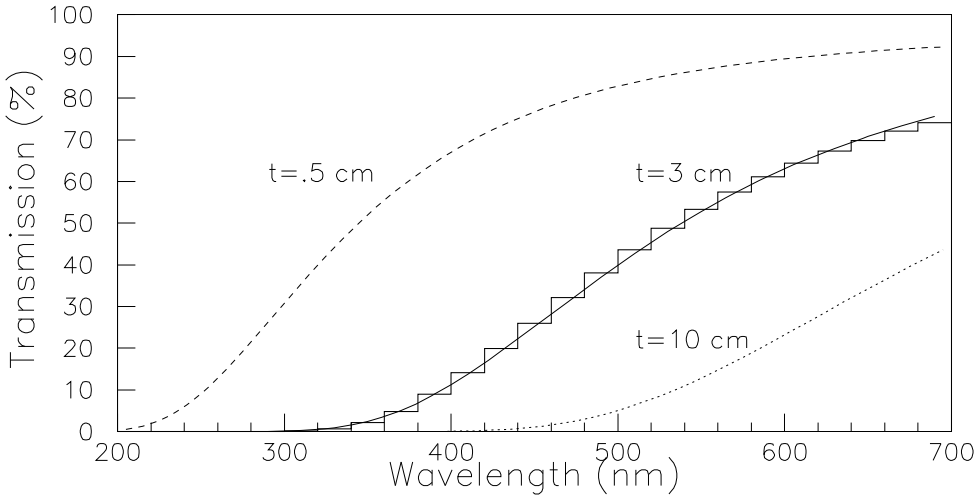

Figure 1: Transmission spectrum (histogram) of a 3cm sample of aerogel. Also shown are a fit to the spectrum, and spectra corresponding to transmission through 0.5 cm and 10 cm of the same material, derived from the fit.

From the small width of the rings that were captured on photo in the 1993 beam tests we can conclude that the uniformity of the index of refraction throughout the material is good.
The wavelength dependence of the index of refraction is not measured. However the ring we photographed in 1993 showed no color fringes, though the behavior of the photographic emulsion may be responsible for the uniform color of the ring. The dependence of n on the wavelength in fused silica is small in the interval 350-500 nm. (xxx Doug verify this last sentence xxx)

4.2 Transmission, scattering and absorption

On a microscopic scale, aerogel is a sponge-like material with typical structure scale length of 3-5 nm. Because this is much smaller than the wavelengths we are interested in, behavior of visible light in aerogel is dominated by Rayleigh scattering, which goes as λ^{-4}.
The transmission spectrum of a sample of thickness L can be parametrized as $T = A * e^{L*C/\lambda^4}$. A and C are what we call the 'Hunt parameters' which describe the aerogel. A is the transmission at asymptotic values of λ, and should be maximally about 94%, the value for a clear piece of glass. The value of C reflects the microscopic properties of the aerogel. To first order it is independent of the index of refraction n. Lower C means better transmission. An example of such a transmission spectrum is shown in the histogram of 1. The thickness of the sample is 3 cm, and the fit gives A=96 and C=184×10^{-4}. Note that wavelengths below 320 nm are completely absent. However in a cherenkov detector, photons are produced all along the path of the particle, and not all photons have to traverse the full radiator thickness. The dashed curve shows he transmission spectrum of light in this sample if only 0.5 cm needs to be traversed. Shorter wavelengths now contribute. Conversely, for thicker samples, the curve moves to the right, and when there is an upper wavelength limit to the response of the readout system (like 550 nm for a PMT), there is a maximum radiator thickness beyond which hardly any unscattered light contributes to the signal,

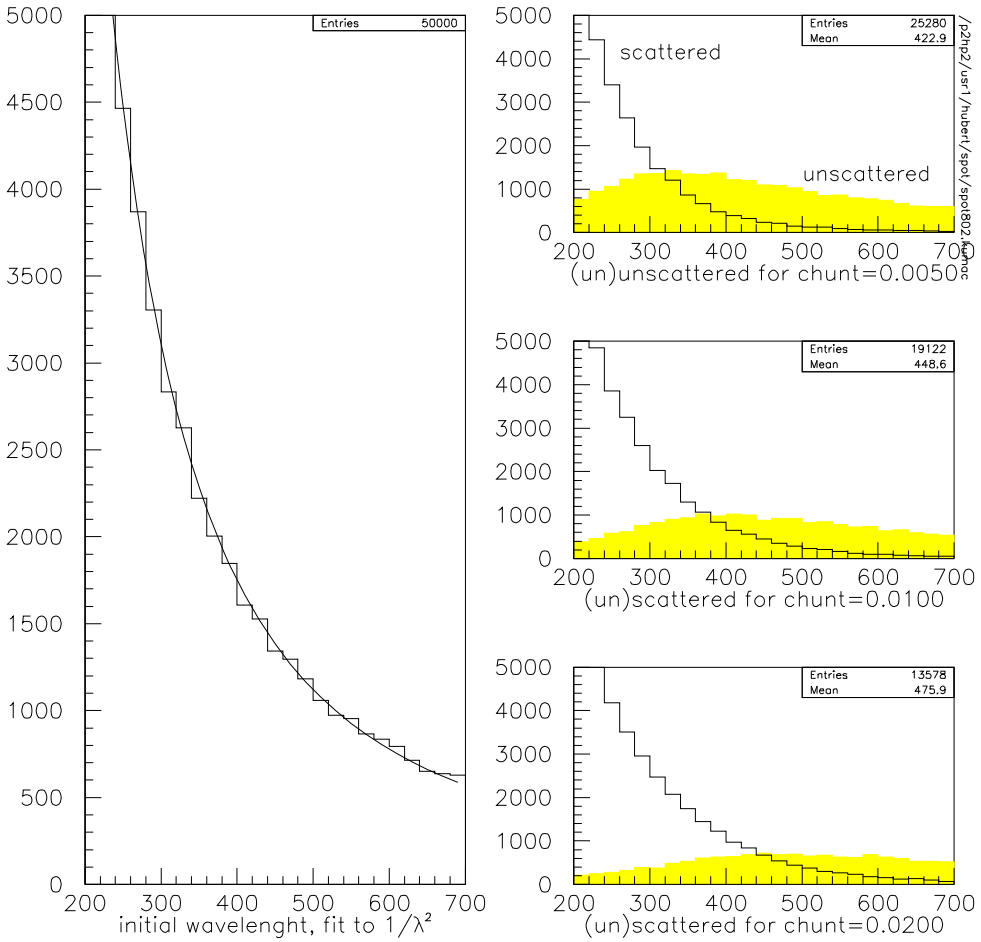

Figure 2: Cherenkov spectrum and spectra of scattered and unscattered photons.

as shown by the dotted curve in figure 1.

The scatterd photons, however, do not vanish, ans some of them may still exit the aerogel in the forward direction. Figure 2 shows on the left the starting cherenkov spectrum, and a fit to λ^{-2}. On the right this spectrum is broken up into two components: those photons that exit the aerogel without scattering, and those that undergo at least one scattering in the aerogel. This breakdown is shown for 3 values of Chunt: 50, 100 and 200 ($\times 10^{-4}$), corresponding to the best aerogel reported in the literature, our first samples from Lockheed, and our aerogel from Airglass, respectively. What one can see is that as the aerogel becomes clearer, the total number of unscattered photons goes up (the statistics printed in the boxes are for the unscattered spectrum), and that the peak of the spectrum moves to lower wavelengths. Still, there is an enormous number of scattered photons in the typical PMT wavelength range of 300-500 nm.

In figure 3 are shown the scattered and unscattered photons that make it to the PMT when one considers only geometrical acceptance; That is, ignoring losses due to reflection, transmission and quantum efficiency. Clearly very few of the scattered ones survive. This is because after a few scatterings, their direction is evenly distributed over 4π, whereas only photons in a small angular range have a chance of survival. The plots on the left-hand side show the raw numbers of surviving scattered and unscattered photons on a log scale, and the ratio, a measure of signal-to-noise at the single-photon level, is plotted on the right-hand side on a linear scale. The crude spline fits show that - not surprisingly - things look better for clearer aerogel. However

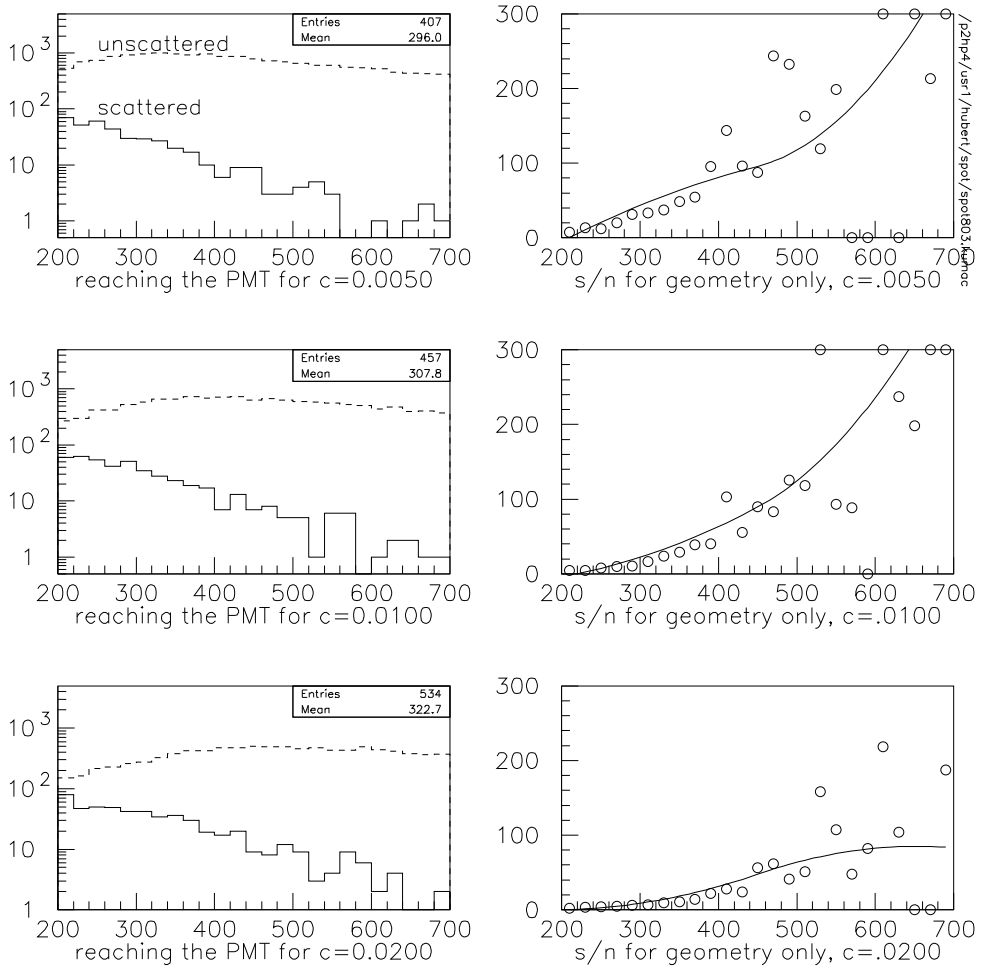

Figure 3: The left-hand plots show the number of scattered and unscattered photons arriving in the focal plane versus wavelenght, and the ratio scattered/unscattered is shown in the right-han plots. The calculations are shown for three values of aerogel clarity.

from the ratio, as well as from the raw 'scattered' distributions on the left of figure 3 we can also conclude that the spectral shifts as we go from bad (chunt=200×10^{-4}) to excellent (chunt=50×10^{-4}) aerogel, are not very dramatic. The plots on the following pages are an attempt to make that more quantitative. Basically a PMT with bialkali photocatode cuts off at the upper end at about 550 nm, and at the bottom at 300 nm for normal (borosilicate) glass, and around 200 nm for UV glass. What I did in 4 is take the spectra from the left of figure 3 and integrate backwards from 550 nm. On the left are the integrals on a log plot, on the right the same plots on a linear scale. From the left column we learn that as you go to lower frequencies, the fraction of noise you pick up increases, and on the middle plot on the right I indicated that by the time you reach 300 nm, you have already collected 82% of all photons, but you can gain 18% by using a UV glass PMT. However, you will pick up more than 18% in noise. It is a bit hard to see in figs 4, so in fig 5 I plot the ratio of the backward integrals. It shows that for the middle sample, the s/n at the single-photon level is 45 if a regular PMT is used, and falls to about half that if a UV glass PMT is used. [The assumption in deriving estimates from the integrals is that the response of the PMT is flat in the chosen frequency ranges. The real gain should be derived from running the full MC containing the proper quantum efficiency and transmission curves, which

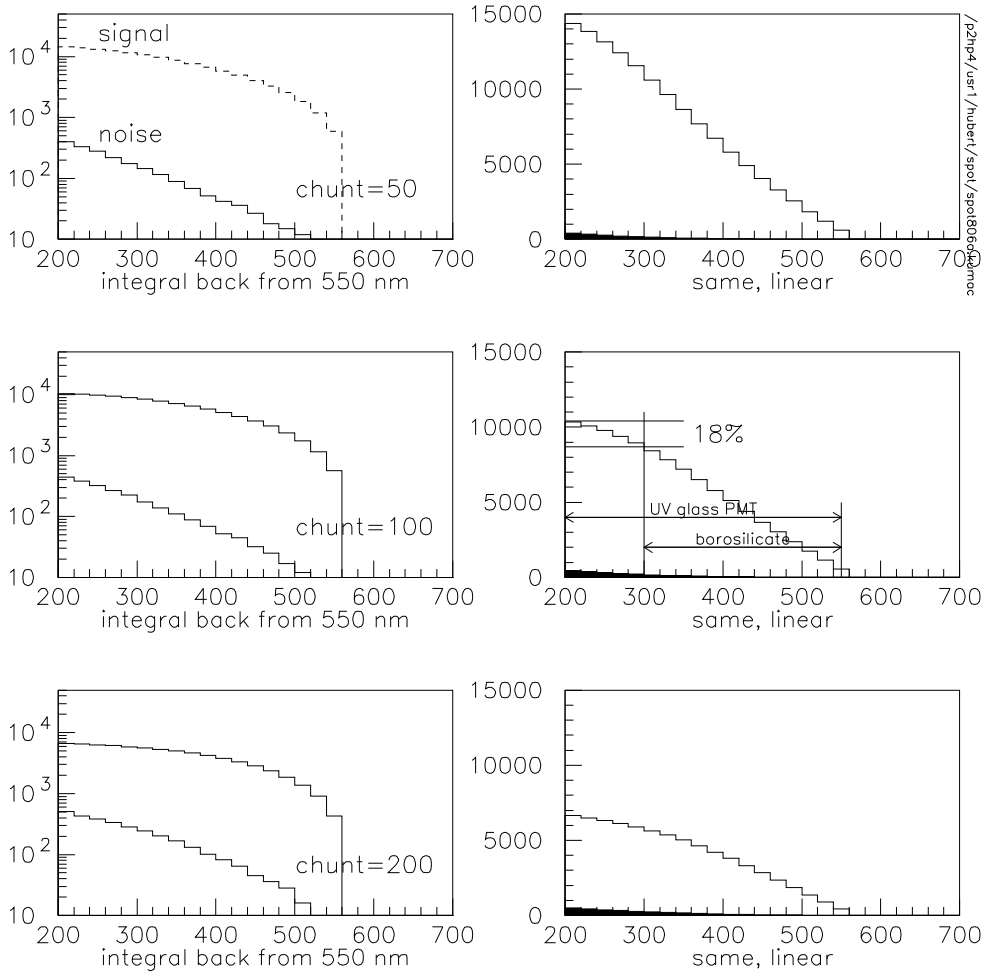

Figure 4: See text

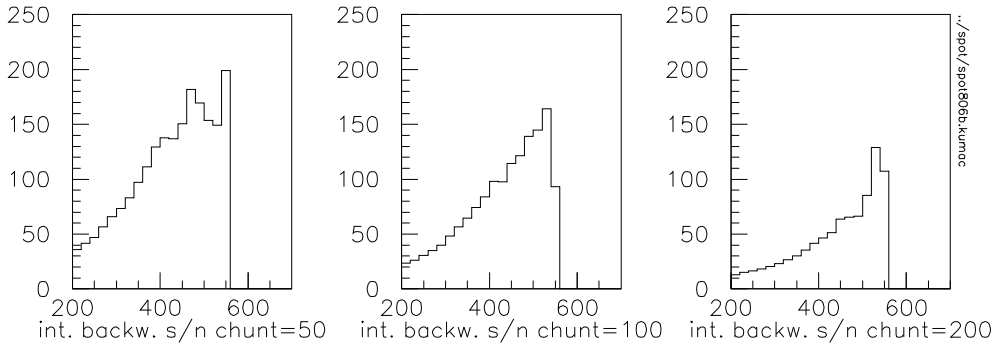

Figure 5: See text

is done below.

Where in the aerogel do detected photons come from? In figure 6 is plotted the z-position in the aerogel (3 cm thick samples) for those photons that reach the PMT. The density peaks at the exit face, presumably because shorter-wavelength photons now have a chance to get out unscattered. To show that effect, the z-position is plotted versus wavelength. At 700 nm, aerogel is transparent and the distribution in z is flat. At z=3 cm, where all photons can get out, the spectrum falls as λ^{-2}.

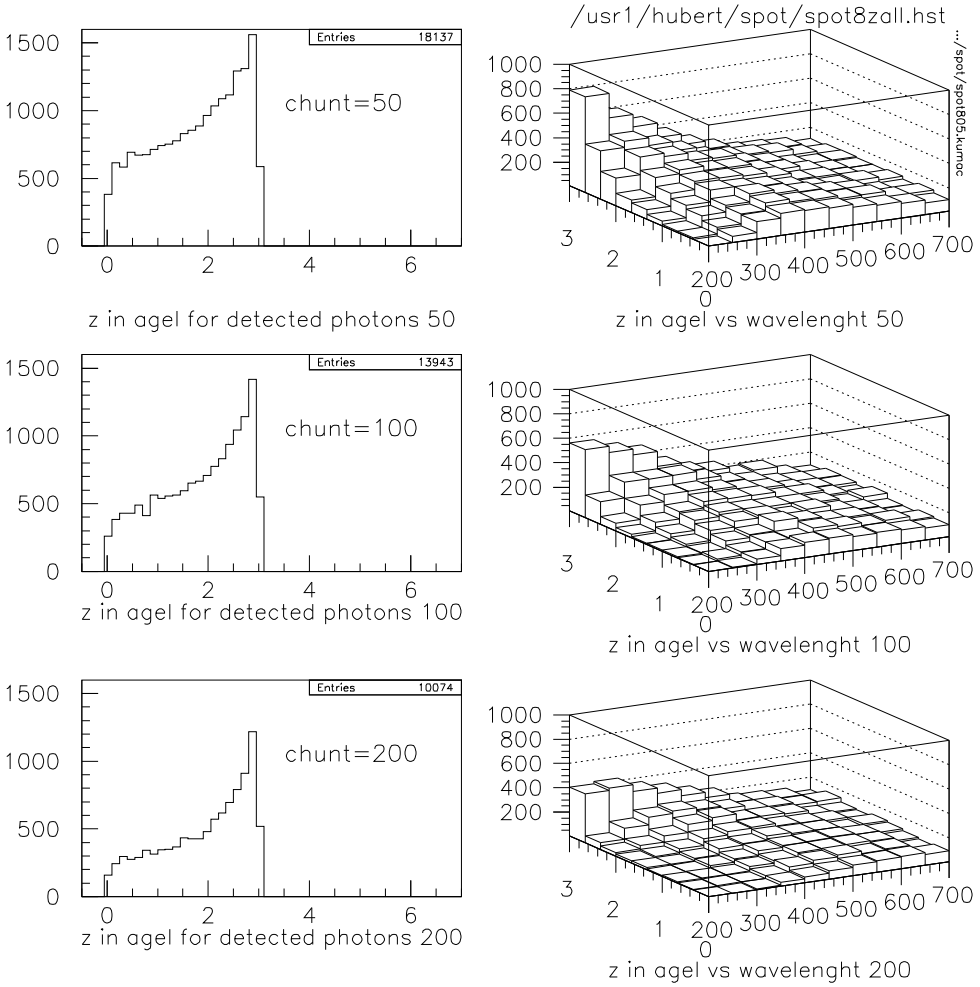

Figure 6: Origin of unscattered photons coming from a 3-cm blck of aerogel. On the left one can see that many come from positions close to the exit surface. On the right-han side onc can see that this dependence is most pronounced for short wavelenghts, but that there is almost no position dependence for the longest wavelengths.

4.3 Optics

Although aerogel has a very low index of refraction, at the edges of most aerogel one can see that the peice is not usually flat, and therefore causes a lens effect there. Although one might think that this effect is too small to consider since the index of refraction of aerogel is so small, it can be a significant effect. For instance, for light at 9° to the normal inside the aerogel (a typical angle for 4GeV kaons), the exit angle will be 9.18° to the normal for $n = 1.020$. If there is a local deviation from a flat exit surface of 10°, the exit angle will be corresponding to a deviation from the nominal position at the focal plane (50cm away) of 1.7mm. We can use this to determine the necessary flatness of the aerogel. In order to keep the deviations at the focal plane to less than 0.5mm, the aerogel must be flat to within 2°.

4.4 Aerogel Production

Aerogel is not a particularly easy substance to manufacture. The material starts out as a gel, with an organic solvent base. If you remove the liquid by simple evaporation, then the surface tension of the liquid will collapse the voids in the material, and no low-density material is formed. In order to prevent the collapse of the gel, the pressures

and temperatures during liquid extraction need to be raised such that the solvent is above its triple point. Then there solvent can be extracted without collapsing the gel. The combination of an organic solvent, high temperatures and high pressures is not without risk. In addition, there is a relation between the desired final density and the speed of liquid extraction which places an effective lower limit on the densities can be reached. In recent years, a two-step process was developed in which the solvent is first exchanged with CO2, and in the second phase the CO2 is supercritically extracted. The two-step process allows better process control. In a final processing step, the aerogel can be baked at several hundred $^{\circ}C$ for many hours, which drives off remaining solvents adsorbed on the aerogel. There seems to be plenty of black magic in each of the steps. See appendix I for a list of manufacurers.

5 Detector Design

The history of the collection optics design is both long and colorful. Rather than discussing the details of all the options which were explored, I will refer the reader to previous notes on the subject in appendix II. The final, optimized geometry is shown in figure 7 with the cover removed.

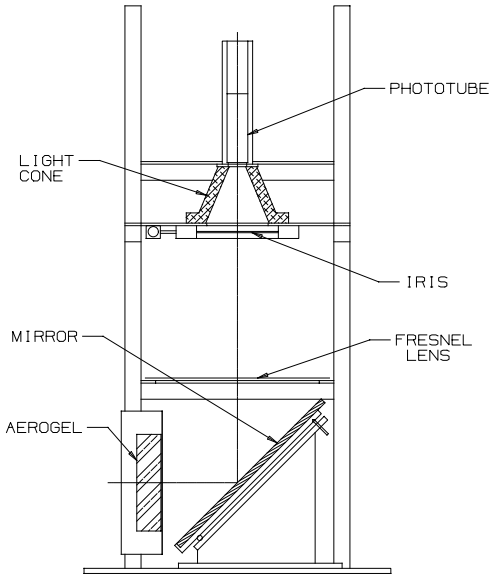

Figure 7: Schematic drawing of the detector as used in the 1994 Pb beam run.

Particles enter from the left and traverse the aerogel, shown as a shaded rectangle. The cherenkov light is reflected off the 45° mirror up to the first fresnel lens. The light is then focussed by the first lens into a ring at the position of the movable iris. The iris diameter can be adjusted so that it passes the kaon ring, but blocks the pion ring. The light from the kaon ring is then collected by a second fresnel lens and a light cone on to a single phototube. Each of these elements will be discussed in detail.

5.1 Mirror

In order to get the collection optics out of the way of the spectrometer path, a thin flat mirror is placed behind the aerogel radiator at a 45° angle. This reflects the light upward so that thicker elements such as the lenses do not cause multiple scattering

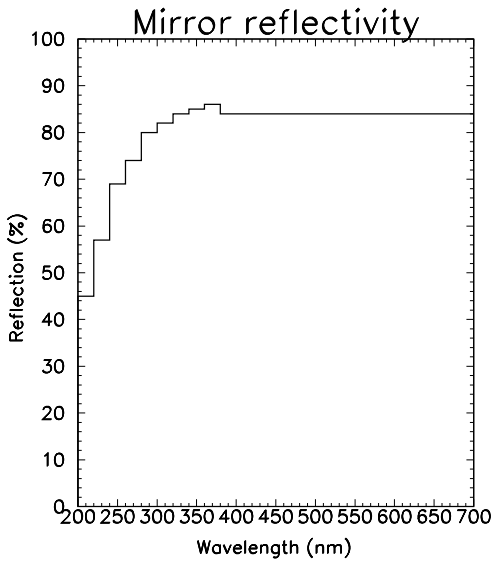

Figure 8: Measured reflectivity of the aluminized mylar mirror.

of the charged particles. This mirror should be as thin as possible while maintaining high reflection and good optical flatness so as to not distort the cherenkov light.

Our first attempt at this mirror was stretched aluminized mylar on a sturdy aluminum frame. The mylar was epoxied to the aluminum frame and then sent to P.A. Clausing, Inc. [2] to be aluminized (at a cost of $200 per mirror). The thickness of aluminization was requested to be 1200 Å, sufficient for good reflectivity. The mirror was not checked for reflectivity until after the 1994 Pb run. We assumed a 90% reflectivity over the entire range of wavelengths (200 - 600nm).

After the 1994 Pb run, the reflectivity was measured at Cern in Andre Braem's optics lab. Figure 8 shows the measured reflectivity curve for the aluminized mylar mirror. The values above 500nm are fixed in the MC and in the figure at a constant value of 84% since Andre did not feel that his apparatus worked well above 400nm and one would expect a near constant reflectivity above 400nm for aluminum.

It was also noted that the mirror seemed to diffuse the light a lot. Light was projected light onto the mirror in a 3mm spot, and 50cm above the mirror he measures the light through a diaphram. When the diaphram was opened from 4mm to 40mm the light intensity went up by a factor of two. This should be investigated further.

5.2 First lens

The final choice for the first element of the focussing optics is a large diameter fresnel lens supplied by Fresnel Optics [3]. The lens diameter is set by the acceptance of particles at the detector position and the distance from the aerogel to the lens (taking into account the flat mirror). The flat mirror is placed as close as possible to the aerogel, and the lens is placed as close as possible to the flat mirror, all done in order to minimize the lens diameter. Since the cherenkov light angle for 4 GeV kaons is approximately 9° and the distance to the lens is 50.7cm, the lens diameter must be 2 x tan(9) x 50.7 + corner to corner acceptance at the front of the aerogel. The lens focal length should be as strong as possible in order to efficiently collect the light onto a small phototube. Based on cost, transmission properties and availability, the properties of the lens which was chosen are as follows:

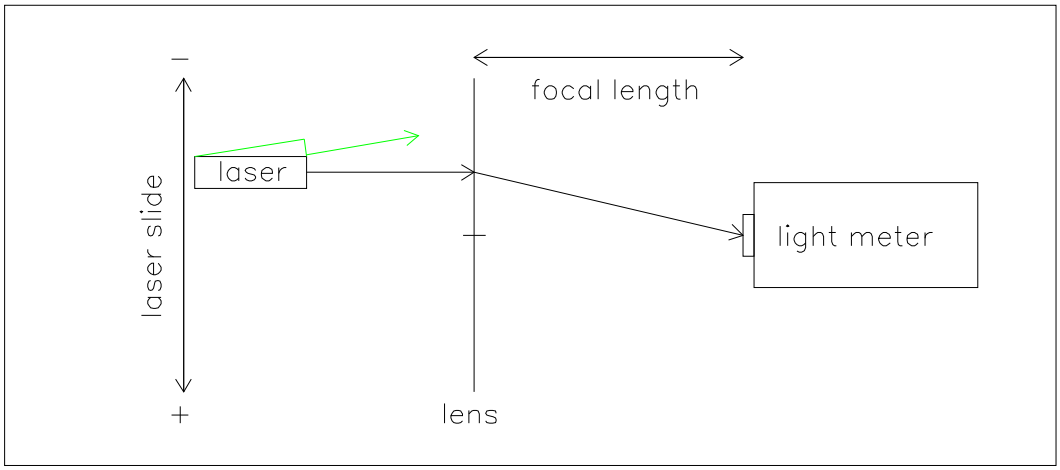

Figure 9: Layout of the apparatus used to measure fresnel losses.

part number = SC2045-UVT
focal length = 39.12cm
active diameter = 45.72cm
facet spacing = 0.508mm
thickness = 2 mm
price = $35.00

The lens was made from a UV transmitting acrylic. The transmission curve for this material was measured through a clear (not lensing) portion of the lens material. The transmission spectrum for this material is shown in figure 13b.

In the original Monte Carlo, the losses attributed to the fresnel lenses were only the spectral transmission losses in the acrylic. The literature also mentioned a 'fresnel loss', presumably due to the fact that rays get intercepted by the vertical facets of the fresnel ridges, but these losses were zero in the center of the lens, and 5% or so further out. This effect was not modeled until recently, when we were searching for explanations for the unexpectedly low signal in the cherenkov counter. We decided to measure the fresnel losses in the lab. The setup is shown in figure 9.

It consists of a small laser which rides along a rail transverse to the output beam. The beam is either normal to the rail or makes an angle of 10° to the normal. The beam strikes the lens, and in the focal plane we either place a ruler parallel to the lens, or a light meter.

In an ideal lens, light coming in parallel to the optical axis goes to the focal point, regardless of where it hits on the lens. This is shown in figure 10a, top trace, which shows that the deviation from the focal point is zero for all values of the radius of incidence. When the light is incident at 10°, there is a small deviation from this ideal behavior, as shown by the points and the bottom trace. The maximum deviation is -7 mm at a radius r=20 cm. These measurements were done with the fresnel ridges towards the laser. If we now flip the lens around and repeat these measurements, a dramatically different behavior is seen, as shown in figure 10b.

For normal incidence, The lens behaves acceptably only for radii less than about 8 cm, but beyond that the light moves away from the focal point quickly. The same striking difference between the two orientations can be seen in the plots for the light

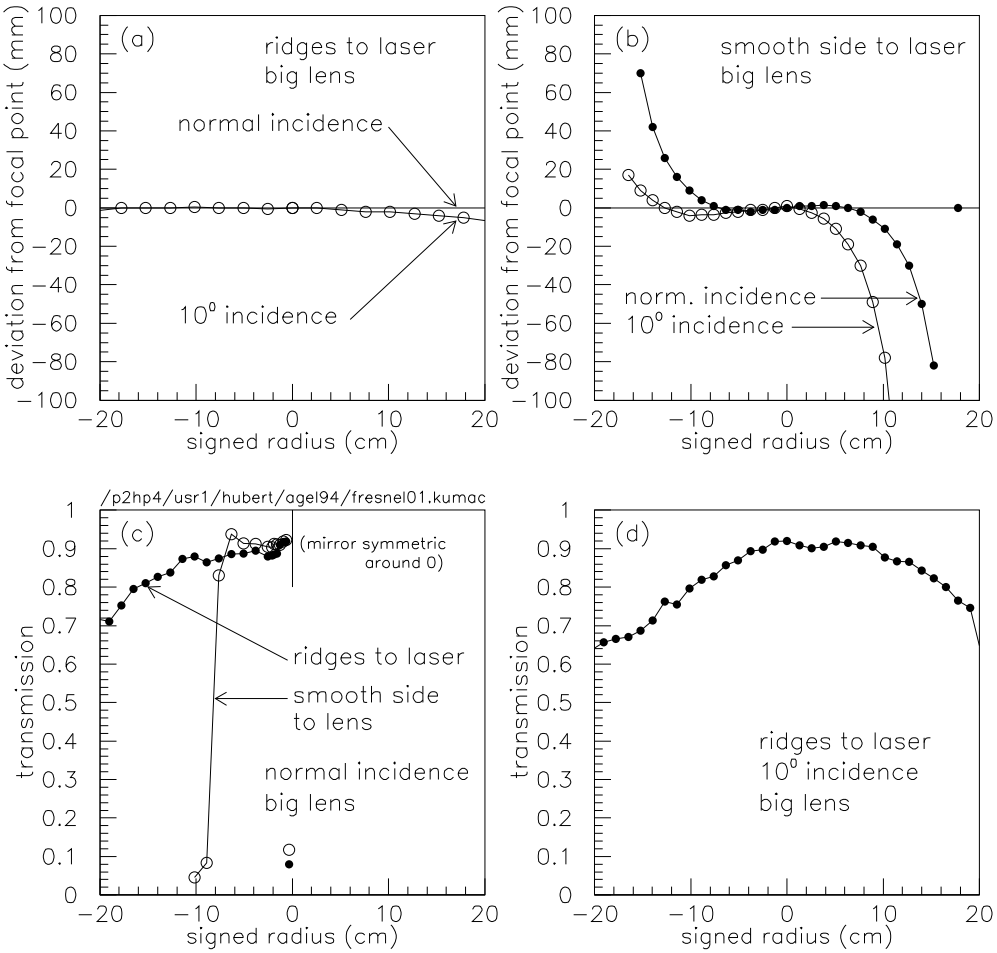

Figure 10: Measurements made on the big fresnel lens.

transmission, figures 10c,d. The solid points in 10c show the fraction of the light that ends up in the focal point, relative to the amount that the light meter reads when the lens is removed, as a function of radius. It starts at about 90% in the center, and drops smoothly to 70% at the extreme radius. With the smooth side facing the laser, however, the intensity drops to practically zero around r=8-10 cm, caused by the fact that the light has moved off the light meter.

Figures 11a,b show the same measurements for the small lens. This lens was the one used in the small test device on the 1993 beam tests, and is also the small lens that sits just behind the iris in the big detector.

Although some small deviation from ideal behavior was not unexpected, these gross failures for the 'backwards' orientation came as a surprise. It turns out that during the 1994 lead runs the big lens was installed backwards, and the small lens was installed correctly.

The behavior of the lenses as shown in figures 10 and 11 were subsequently modeled in the MC by parametrizing the observed effects. In a parallel effort, we used the lab setup to measure the angle of the fresnel facets as a function of radius. With this knowledge, a 'microscopic' simulation of the lens was written, where each ray was traced in detail through the fresnel surfaces. This description also reproduced the benchtop data.

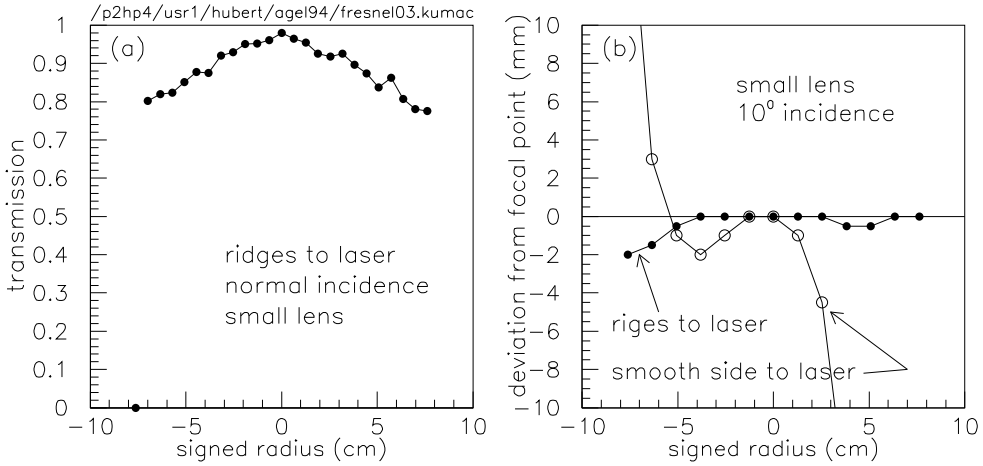

Figure 11: Measurements made on the small fresnel lens.

5.3 Iris and controller

At the focal plane of the first lens, an adjustable iris is placed in order to block the pion ring and allow the kaon ring to pass. The iris diameter must be able to be adjusted externally to allow for fine tuning. This tuning is necessary since the exact index of refraction of the aerogel is not easily determined. Also, in order to maximise the efficiency of the two-kaon trigger, one would want the ability to open the iris diameter until the maximum tape speed is reached (See section 8). The iris was purchased from Edmund Scientific [4] and has the following properties:

part number = D70,895
maximum diameter = 225.0mm
minimum diameter = 9.9mm
number of blades = 20
price = $420.75

In order to adjust the iris without opening the detector, a six-volt motor is attached to a ball screw assembly which turns the iris adjuster pin. Between the motor and the screw is a 10-turn potentiometer (0-1000 ohms). A controller was built which both reads out the potentiometer and supplies the 6V power to the motor. The potentiometer is read out through two banana plugs on the top front of the controller. The power to the iris adjusting motor is turned on by a toggle switch on the bottom front of the controller. Another toggle switch determines the direction, out or in, for the adjustment, and a push button activates the motor. Contact switches on the iris mount limit the motion of the ball screw nut. In order to convert from potentiometer reading to iris diameter, measurements of the iris diameter were taken as a function of potentiometer reading at the controller. This was done with the detector in its final position and the controller in the NA44 counting house in order to take all cable resistance into account. The results are shown in figure 12 and are parameterized as

$$diameter = 95.99 + 0.0834 * (potentiometer) + 1.3^{-5} * (potentiometer)^2 \qquad (4)$$

Also shown in figure 12 is the difference Δd between the calculated dependence and the measured values. It can be seen that the parameterization is good to about 0.5 mm.

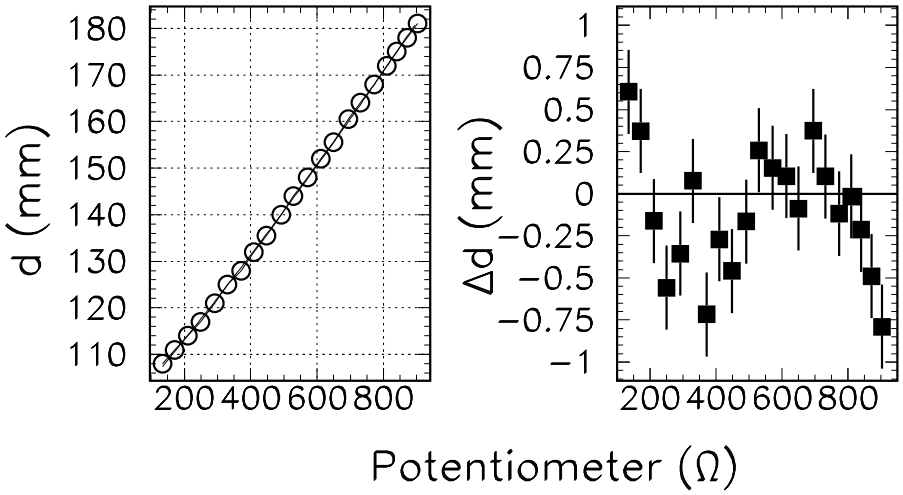

Figure 12: Measured diameter of the iris as a function of potentiometer reading at the controller in the NA44 counting house (left). Also shown is the difference between the calculation and the measured points (right).

In addition to the movable iris to define the outside of the kaon Cherenkov rings, there is a fixed circular mask blocking light center of the opening. It has a diameter of 9.5 cm, which is just smaller than the Cherenkov ring of a 3.5 GeV kaon, the lowest momentum expected at the 4 GeV setting. Since no light at smaller diameter can belong to a kaon signal, we can reduce the pion background by blocking this area and intercepting scattered photons there. This mask is actually attached to the second fresnel lens.

5.4 Second lens and light cone

Once the light is past the focal plane, all that remains to be done is detect it. Since we had a very efficient 1.5" phototube in hand, The task is to collect light which is in a ring of about 14 cm diameter and has an angular spread of about 18° onto a circle of 3.7 cm diameter.

guide connects the hole and 1.5" PMT. The ray that is drawn shows a problem with a geometry like this: there are rays that get bounced too many times, and eventually come back out the front and are lost. The solution chosen was to place a lens in front of the cone, thereby tipping incoming rays into the direction of the PMT. This reduces the average number of reflections in the light cone, and thus reduces the number of photons lost. The height of the cone was chosen to maximize the number of photons reaching the PMT face.

The second lens was also a fresnel lens supplied by Fresnel Optics [3]. This lens was chosen based on cost, transmission properties and availability. The properties of the lens are as follows:
part number = SC247-UVT
focal length = 14.73cm
active diameter = 15.24cm
facet spacing = 0.508mm
price = $18.00

Outside of the active diameter is clear acrylic. The pion rings are larger that this diameter, and thus rays from pions are not refracted. As a result, light from pion rings is not collected efficiently by this lens/cone combination.

This configuration, consisting of a lens and a cone, can be optimized for each PMT diameter. Also, for the 5" tube the placement of the tube itself becomes arbitrary as the tube face is almost the same diameter as the cherenkov ring. In table 5 I show the optimal arrangements for tube diameters ranging from 1" to 5", assuming 90% reflectivity for the light guide surface.

PMT		outer cone		inner cone		photons	mean#	with 90%
size	y-pos.	y-pos.	angle	y-pos.	angle	at PMT	refl.	refl.
1.0"	85	88.9	15.4	83.0	12.2	6834	2.8	5099
1.5"	92	101.0	10.7	91.0	8.8	11492	2.4	8887
2.0"	81	89.8	15.0	none		11893	1.4	10261
5.0"	69	84.6	18.3	none		11916	0.6	11186

Table 1: optimized light guides for various PMT diameters

Note that for tubes below 1.5" there is a fall-off of the number of photons that can reach the PMT even with 100% reflectivity. Also, the effect of the number of bounces in the light cone when the reflectivity is set to 90% becomes worse for smaller tube diameters. These results strongly argue for choosing as large a PMT as possible.

6 Detection of light

6.1 Single detector

In figure 13a is shown the quantum efficiency folded with the window transmission for a bialkali photocathode with borosilicate glass (400K), UV glass (400U) and quartz (400S) windows (taken from the Hamamatsu catalog). Figure 13b shows the transmission we measured for our acrylic lens. If I run the full simulation (with a 2" PMT and a simple light cone, more details below), and use 3 cm aerogel with C=100*10-4, I can exchange the PMT windows and see if I gain anything. The results are:

	acrylic transmission	
tube type	normal	shifted
400K	425	406
400U	430	469
400S	430	454

Table 2: Number of photoelectrons for 3 types of PMT entry window materials, and 2 different transmission spectra for the acrylic fresnel lens. (Arbitrary normalization)

One can see that 1% in signal can be gained by switching from borosilicate glass to UV glass or quartz. Note that the increase is governed solely by the cutoff of the acrylic spectrum. A shift of the absorption spectrum to the left by 20nm (one bin in figure 7) results in a 10% gain.

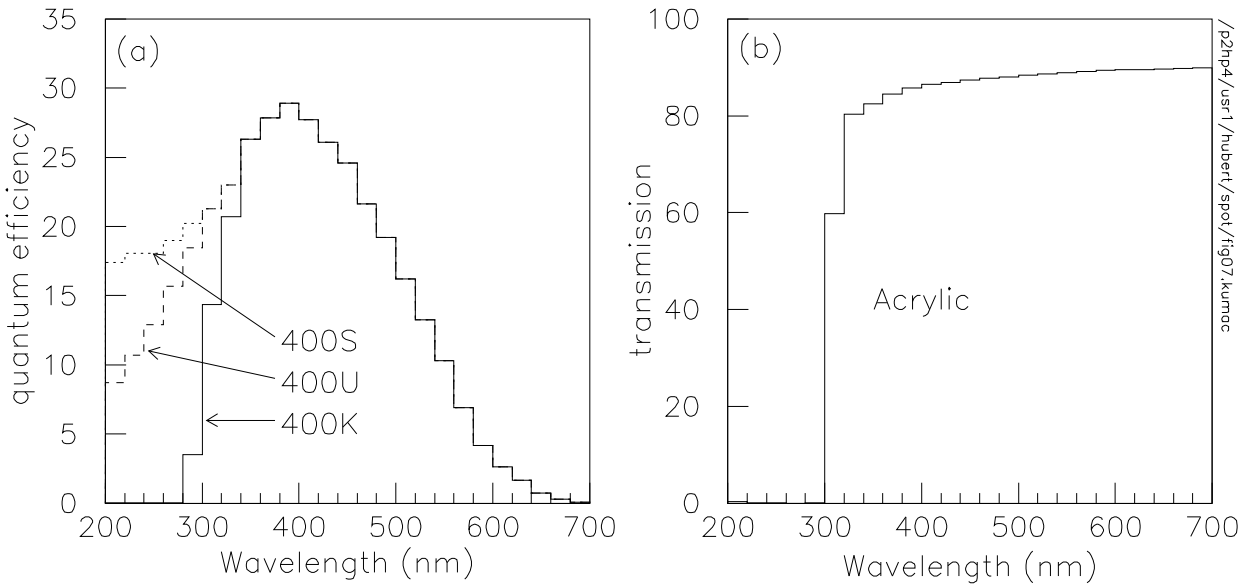

Figure 13: Quantum efficiency of the EMI9125 PMT (a), and transmission spectrum of the UV-acrylic of the fresnel lenses (b).

6.2 Multiple detectors

There are two advantages of smaller using multiple phototubes at the ring plane. First, it is easier to place them closer to the ring since the magnetic shielding has to extend past the cathode surface roughly 1.5 times the phototube diameter. Secondly, if the average occupancy of photons in any one detector is below 1.0 for a two-kaon event, then one can put a threshold on the phototubes just above noise and count the number of phototubes above threshold. This gives some gain in resolution since you no longer have to consider the width of the n-photon peak.

The disadvantage is that you need fifteen phototubes instead of one, and you also have to carefully set the threshold for each one (gain matching).

6.3 Avalanche photodiodes

Another option for photon detectors would be avalanche photodiodes. The big advantage of these detectors is high quantum efficiency. The drawbacks are high cost and the need for the development of driver circuitry and a preamp.

7 Alignment

Because of the sensitivity of the ring position to the alignment of the detector with respect to the spectrometer axis, great care must be taken to align this detector properly. For the 1994 Pb run, it was aligned in the following manner:

7.1 Internal alignment

For the internal alignment, what is important is that a ray passing through the center of the aerogel, parallel to the base plate, and perpendicular to the aerogel, strike the center of all elements to within 1mm. This internal alignment was accomplished by:

1. Mount crosshairs at the front and rear of the detector at the same height (beam height = 21.35cm from base plate) and in the exact middle between the supporting vertical extruded aluminum posts.

2. A laser was then placed in front of the detector such that the laser beam hit both crosshairs (with the 45° mirror removed). This then defined a horizontal centered beam.

3. The mirror was then mounted on its support, which was machined to an angle of 45° with respect to the base plate. This is not a critical step as there are other elements which can be adjusted if the mirror angle is not exactly 45°.

4. The laser beam is now reflected up at 90° with respect to the base plate, and with the first lens removed, should hit the center of the second lens. The mounting plate for the second lens was adjusted so that this was so.

5. The second lens mounting plate was adjusted for the correct height to put the iris in the proper place.

6. The first lens was installed and centered on the laser beam. The mounting plate for this lens was also adjusted to put the first lens at the proper height.

7. Since the light cone and the phototube are mounted centered on the second lens, they needed no further alignment.

This internal alignment process was done carefully both at the PS hall before the detector was taken to the North Area, and also again, after mounting in its final location in the NA44 spectrometer. The internal structure of the device is such that none of the elements moved during transportation..

7.2 External alignment

Once the internal elements are aligned to the center beam properly, the detector must be located on the spectrometer such that its center line is the center line of the spectrometer. For the 1994 Pb run, this was accomplished in the following manner:

1. With the detector placed on the mount with the tophat off, the surveyors could see the two crosshairs which defined the center line. The mounting plate was then raised until the center line was at the same height as the spectrometer axis.

2. With the detector now sitting at the correct height, the surveyors set up their scope so that it was parallel to the beam line. measurements were then taken from the center line to the scope line and the angle adjusted so that the measurement from the front crosshairs was the same as the measurement from the back crosshairs. This adjustment places the detector parallel to the spectrometer axis.

3. In order to make sure that the center line of the detector was not offset from the spectrometer center line, a thread was run from the center of the last quadrapole exit face to the center of the entrance window of C1. (The mirror was removed without affecting its alignment for this operation.) The left/right displacement

of the detector was then adjusted until this thread touched both crosshairs. This is done by sliding the entire device, while the mounting bolts are still loose. These bolts have enough clearance to allow this

4. Step two was then repeated to crosscheck the external angle alignment.

It should be noted here that the analysis of the 1994 Pb beam data has demonstrated that the alignment was done properly to a high degree of accuracy. This will be discussed further in that section.

8 Trigger

This detector will add another condition for a valid trigger on top of the existing spectrometer trigger. For a kaon pairs run, it should provide a positive signal that two kaons were in the spectrometer acceptance regardless of the number of pions present.

$$\frac{1}{N_{accepted}} = \frac{1}{N_{presented}} + \frac{1}{600} \tag{5}$$

A 1% target (0.5mm Pb) and a beam rate of 5M/burst, gives 50,000 events per burst. Using RQMD multiplicities, 185 of these events are two or more kaon events. If we had a perfect two-kaon trigger, equation 5 tells us that we could only accept 141 or 76% of them. With half of the beam rate, we would have 93 two-kaon events, and accept 80 of them or 86%.

9 Analysis of the 1994 data

For the lead run, we had obtained aerogel from the Jet Propulsion Lab (JPL). The three pieces measured 9.1x9.1 cm, and were 2.5, 2.5 and 3.0 cm thick. This means that there was a horizontal seam in the center, and there were many interfaces to traverse for photons originating early along the track. The index of refraction of each piece was determined by measuring its density. All pieces were found to have n=1.0211$\pm$0.0004.

During the lead run, the aerogel counter was read out for all runs, although it was never in the trigger. For runs 3287 through 3335, the iris was changed before each run in order to collect data on the behavior of the device. This is shown in figure 14.

These runs were 4 GeV pion pair runs, most of them vertical. In order to get a sample of kaons and pions from these tapes, we make cuts on the C1 signal and the mass^2 as shown in figure 15. In this plane, kaons are defined by $0 < m^2 < 0.5$ GeV^2 and $0 < C1 < 200$ ADC channels. Single pions are defined by $-0.5 < m^2 < 0.1$ GeV^2 and $200 < C1 < 550$ ADC channels. Clearly there are not many kaons in the plot.

Next we project all tracks to the aerogel, as shown in figure 16 for a vertical run.

The aerogel was made up of square blocks such that there was a seam in the horizontal center plane. Tracks are accepted in our analysis if they fall inside one of the 2 squares in the figure, such that they are away from the center seam and from the outer boundary.

For vertical runs, momenta for a nominal 4 GeV setting range from 1 to 15 GeV. For these runs, the momenta were restricted to the range 3.5-5 GeV (the range for the 4 GeV setting).

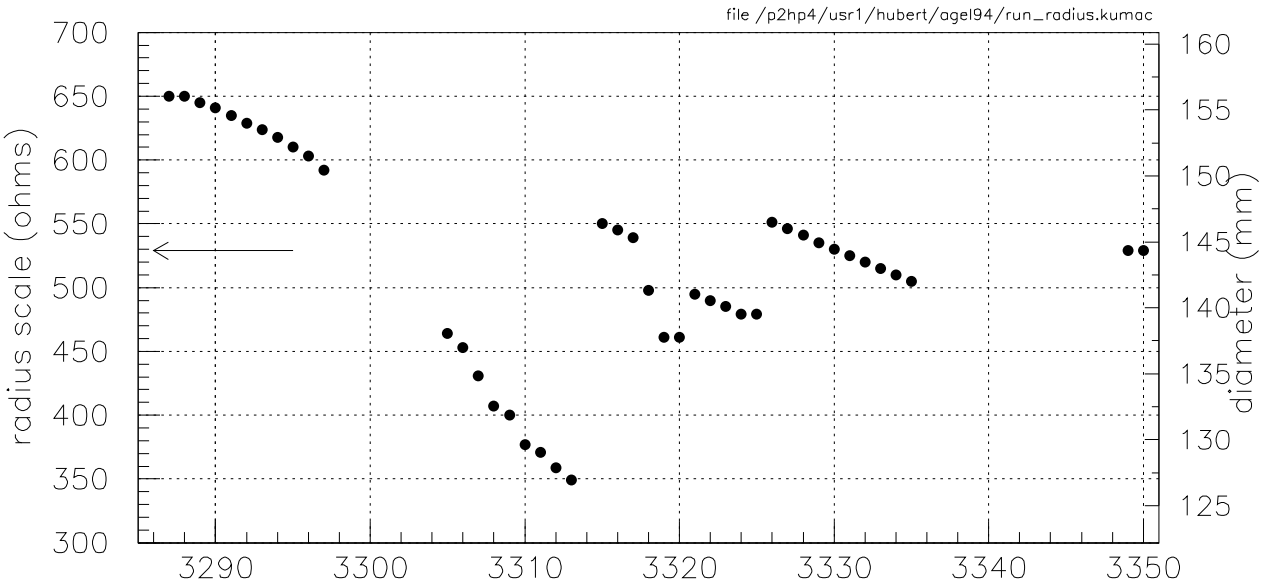

Figure 14: Overview of the available data: the radius of the iris is plotted versus run number. All are at 4 GeV. All are vertical except for 3330-3335. All runs shown are pi pairs, except for 3349-3350, which were K/p singles. The arrow indicates the nominal iris setting.

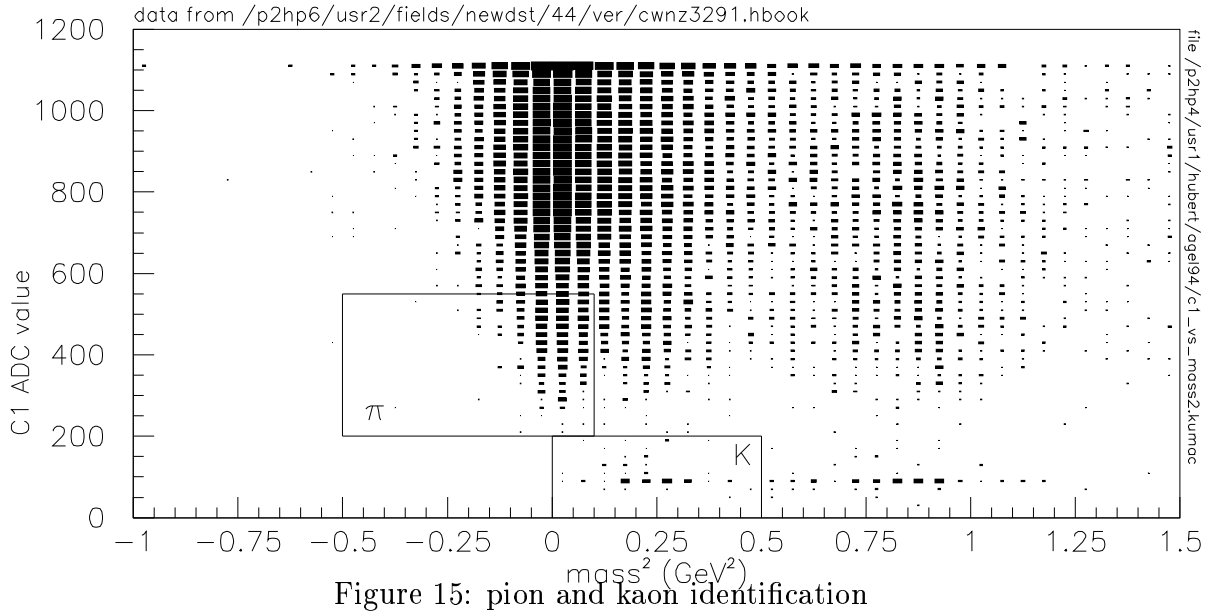

Figure 15: pion and kaon identification

We now plot the aerogel ADC distribution for all tracks (figure 17a), for kaons (17b,c), and pions (17d,e). In 17a, one can clearly identify the pedestal and the 1-photoelectron peak, and do gaussian fits to determine their widths and means. Using these values, one can fit the kaon and pion distributions. Since the only free parameters left are the mean number of photoelectrons and the overall normalization, good fits can be obtained even when statistics are low. Note that since zero-bins need to be accounted for in the fits to the kaon spectra, a maximum likelihood fit must be done. Two other methods were used to determine the mean number of photoelectrons: a number can be derived from the number of entries in the zero-peak and the number of entries above the zero-peak (17c,d). A third method simply calculates the mean of the entire distribution. The three methods give consistent results, which indicates

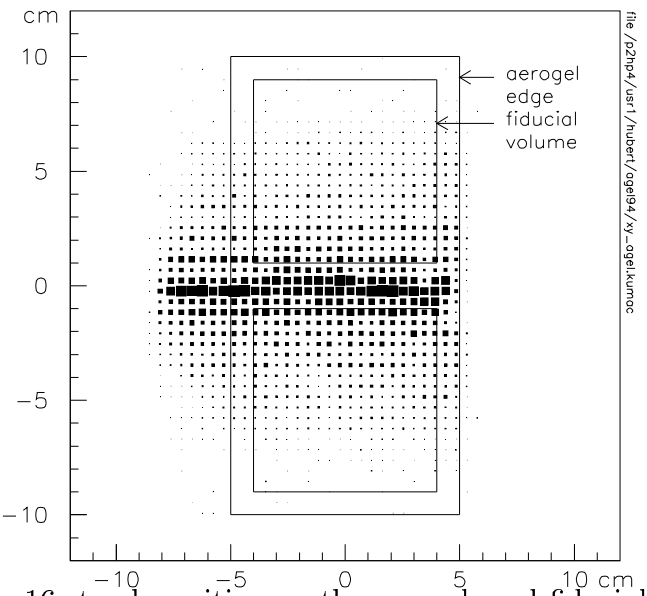

Figure 16: track position on the aerogel, and fiducial cuts

that the kaon sample does not contain a significant pion contamination and vice versa.

Figure 19 shows the combined results for 31 runs. On the horizontal axis is the potentiometer reading that is attached to the iris. The corresponding radius in centimeters is plotted on the axis at the top. On the vertical axis is the mean number of photoelectrons from the fit.

What do we expect to see? Lets first look at the pion plot, figure 19b. In the absence of Rayleigh scattering in the aerogel, this should read 0.0 until the iris opens up far enough to accept the pion cherenkov ring. However, the scattering will cause photons to end up in random locations in the focal plane of the device. In the center of the focal plane, where the iris is placed, there also is a black paper disk with a 4.75 cm radius. Thus the area through which random photons can reach the PMT would be zero at an iris radius of 4.75 cm, and rise roughly linearly with iris radius. This is indicated by the line which is a good fit to the pion data up to r=7 cm. Pion cherenkov rings start at about r=7.3, and we expect a rise in signal starting at that point. However, the active area of the fresnel lens in the focal plane ends at r=7.6, indicated by the vertical line. Beyond that radius, there is clear acrylic, and photons passing through that area are collected very inefficiently by the cone, as they have to make more and more steeply inclined reflections, many never reaching the PMT. Therefore we are not surprised to see a small signal for r> 7.6.

For the kaons (figure 19a), the cherenkov ring maximum is expected at around r=7.2 cm, indicated by a short line segment. Beyond that, the signal should not increase with increasing iris aperture. Below this radius, I show a line that scales the signal by the integral of $\sin(\theta_c)^2$ up from a radius of 4.75 cm. This is a crude calculation that assumes a flat momentum distribution.

Qualitatively, the signals for pions and kaons show the expected behavior. Based on this, we can rule out several hypotheses for the observed low number of photoelectrons in the lead run. First, there are no gross misalignments. If the device had been misaligned, the pion ring would have cut into the iris aperture, sharply increasing the slope of the pion signal well before r=7.3 cm. In the kaon plot, there seems to be a rising trend followed by a flattening out of the data. From the location of the kink one can derive in principle the kaon ring radius, and from that the index of refraction of the aerogel. This is a crude measure, but the kink is roughly where we expect it.

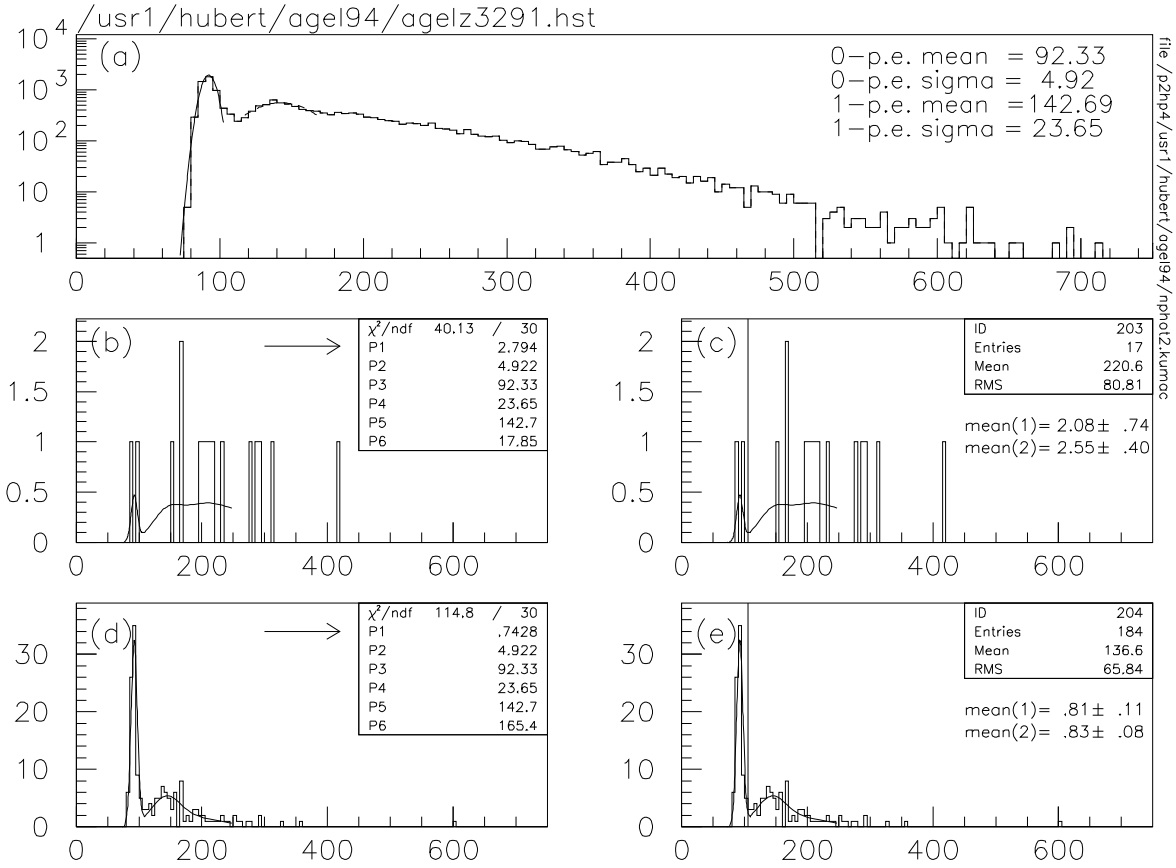

Figure 17: Aerogel Counter ADC distributions for all tracks (a), and for kaons (b,c) and pions (d,e). Fit parameters except normalization and mean number of p.e. are derived from 2 gaussian fits to the top distribution. Two-parameter fits are shown for the kaon (b) and pion (d) distribution to determine the mean. On (c) and (d) the results from two other methods are shown (see text). The three measurements of the mean are consistent.

As a further check on the geometry, I plotted the mean number of photoelectrons for kaon tracks inside a small window of acceptance, and move the little window across the aerogel. Thus we hoped to be able to see the aerogel edges. The results are shown in figure 20.

Ideally, these scans should be flat, with a drop over the range of 4 cm (the width of the window), at the edge of the acceptance. The top scan in particular shows no such plateau.

In the next section we attempt to reproduce these data both quantitatively and qualitatively using a Monte Carlo simulation code.

10 Monte Carlo studies

The Monte Carlo simulation code for this detector has grown and changed along with the detector. Its present state is quite complete. The Monte Carlo begins by taking real track positions and angles from experimental data (1994 Pb runs both horizontal and vertical with no jaws) and creating an event by calculated (RQMD) pion ($< m > = 1.35$) and kaon ($< m > = 0.135$) multiplicities. For each track, it creates photons randomly along the path of the charged particle in the aerogel,

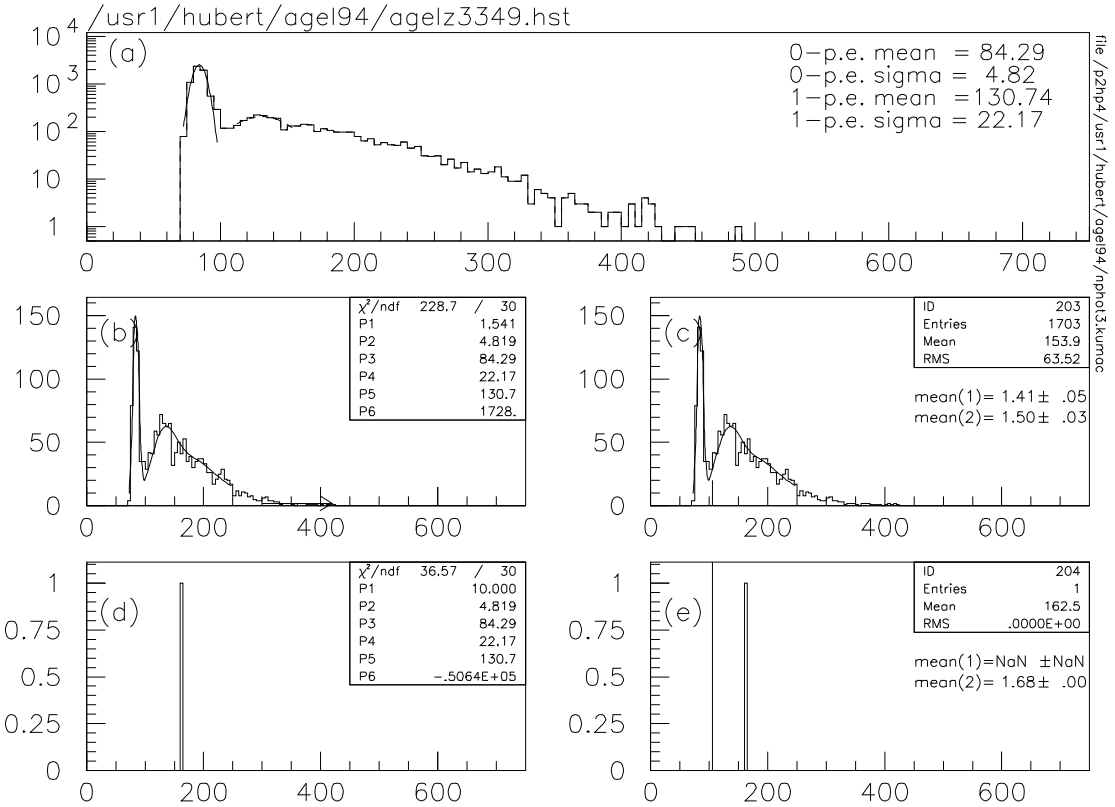

Figure 18: Same as the previous figure, but for a kaon run.

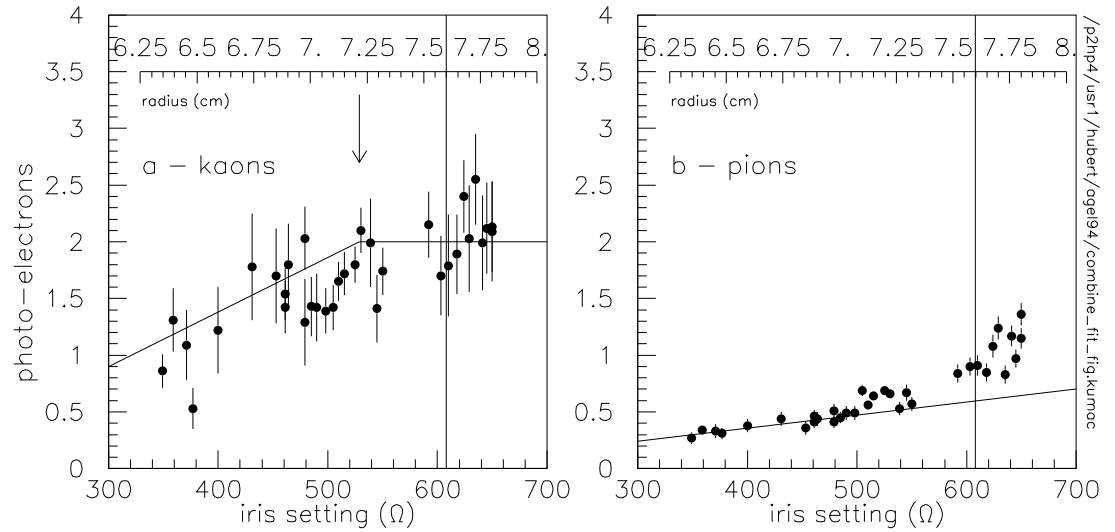

Figure 19: The mean number of photoelectrons seen for kaons and pions, versus iris radius.

calculating its angle from equation 1 and choosing its wavelength and position along the track based upon the distribution given by equation 2. In order to save computing time, the wavelength is then folded with the measured transmission probabilities for the fresnel lenses, the measured reflection curve of the flat mirror, and the advertised quantum efficiency curve of the phototube. If the photon passes these tests, it is folded with the transmission curve for aerogel to see if it would scatter. If it does, it is followed through the aerogel until it is either blocked, or exits the back face of the aerogel. All photons exiting the back face of the aerogel are then tracked through a very accurate simulation of the detector geometry. Photons that reach the PMT

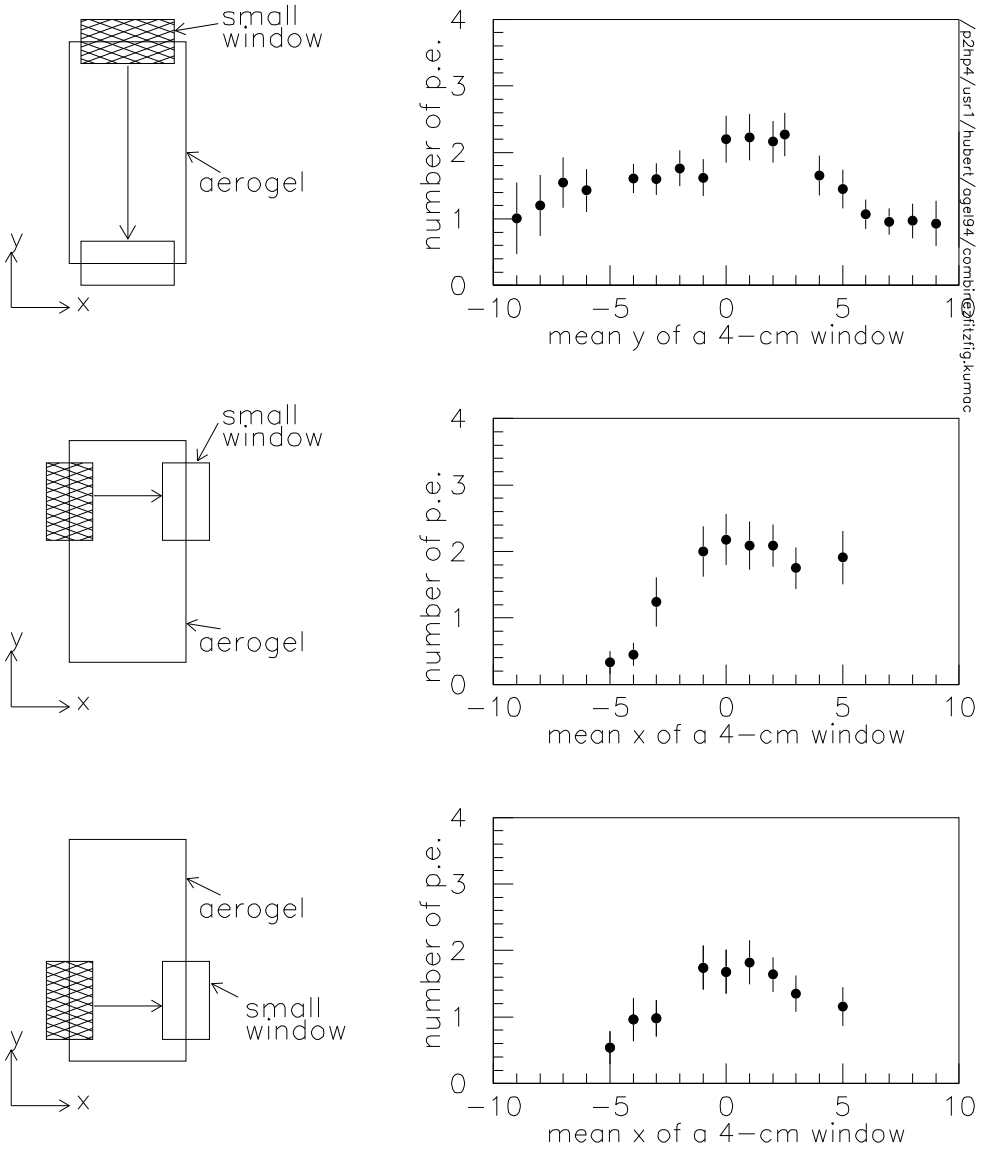

Figure 20: The mean number of photoelectrons seen for kaons in a small subsection of the acceptance.

are also checked to see how many bounces (n) they incurred in the aluminum light cone and folded n times against the aluminum reflectivity curve. The number of photoelectrons (photons are already folded with the PMT quantum efficiency curve) are then counted for each track.

We ran the program to see if it could reproduce the results of figure 19. The results are shown in figure 21. The data are reproduced both qualitatively and quantitatively. Note that the lines on the figure are merely copied from figure 19, and are not fits to the MC calculations.

We also ran the MC to see if it could reproduce the position sensitivity of figure 20. Those results are shown in figure 22. Note that in the MC, the aerogel has an acceptance of 20x20 cm, whereas in the data of figure 20, the aerogel is only 10x20 cm. The dependence on x-position (bottom plot) in this simulation is stronger than on the y-position (top plot). This is due to the angular spread of the tracks in the x-plane, which is virtually absent in the y-plane. This effect can be compensated for by adjusting the y-position of the iris.

For reference, the log file for one of the MC runs (iris diameter = 7cm) follows:

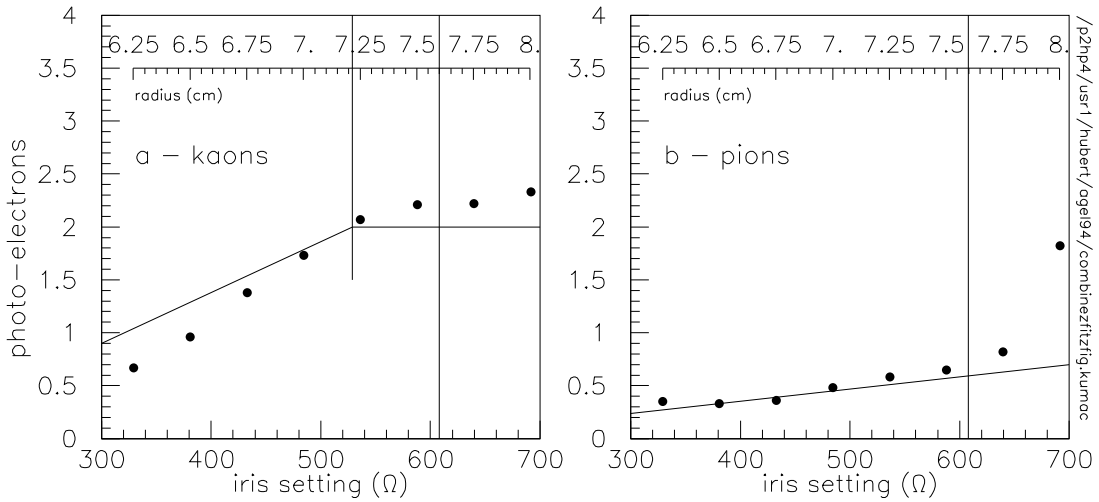

Figure 21: Mean number of photoelectrons seen for kaons and pions, versus iris radius, as calculated by the Monte Carlo simulation. The lines to guide the eye are

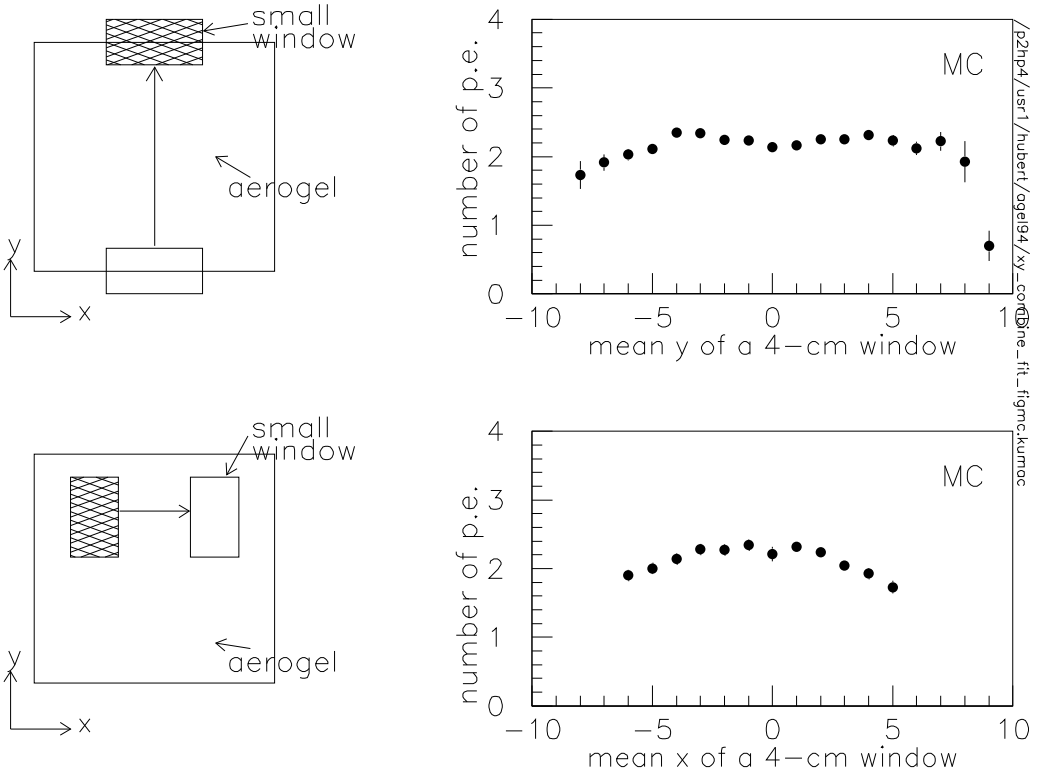

Figure 22: Mean number of photoelectrons for kaons inside a small window of acceptance.

```
xp,yp,zp   (x,y,z of particle) +-10 cm    =   .00     .00     .00
thex,they                   +-3 degrees   =   .00     .00
type (1=e,2=pi,3=k,4=p),  pnom            =  3.00    4.00
zblock,blocks,index (thickness,#blocks,n) = 2.700   3.000   1.021
ppcm (event fraction)       1.0           =  1.00
xflat (x,y,z of flat mirror center)       =   .00     .00   27.90
rflat (s,u,v of flat mirror center)       =   .00    1.00   -1.00
x1lens (x,y,z of 1st fresnel lens)        =   .00   22.80   27.90
r1lens (r-vector of 1st fresnel lens)     =   .00  -39.12     .00
```

```
xcone (x,y,z of cone apex)                =   .00   96.50   27.90
rcone (direction of cone axis)            =   .00   -1.00     .00
cone_angle (half-angle of cone)           = 15.05
xhole                                     =   .00   65.40   27.90
rhole                                     =   .00    7.00     .00
mask (radius of disk in the center)       =  4.75
r2lens (r-vector of 2nd fresnel lens)     =   .00  -14.73     .00
xkdet (cone height=21.2 cm)               =   .00   87.92   27.90
rkdet (direction and diameter of PMT)     =   .00    4.60     .00

nevents         =   100
n_pi            =     1   (Note n_pi and n_ka are ignored
n_ka            =     1    when multiplicity is set to 0.)
multiplicity    =     2    Mult=0 means throw poissons
p_scale         =  1.00
ahunt,chunt     =  1.0000   .0185
1Kcut, 2Kcut    =    800.0  1200.0
PMTname         = EMI9125
HPpath          = /p2hp6/usr1/fields/spot/
VAXpath         = fdata:
file name       = 4gev_hor.hbk
Al reflection from   ALUMINIUM
lens transm. from    FRESNEL3
maxrays         =    50000

Status of: garbage spectra fast rattle
             0       1     1      1
                        also valid: go, help, show, quit, run
Opening file :/p2hp6/usr1/fields/spot/4gev_hor.hbk            ...
Spectral range: 200.-700.
A'gel n, thickness, #blocks, A,C: 1.021  2.7  3.0   1.000    .019
Found spectrum for: ALUMINIUM reflectivity :
Found spectrum for: FRESNEL3 : fresnel at 0 degrees with the
Found spectrum for: EMI9125 : factory spectrum

 -6 - photon did not make a photoelectron          24318
 -5 - absorbed in the light cone                     28
 -4 - absorbed in the 2nd fresnel lens             5781
 -3 - absorbed in the 1st fresnel lens            31820
 -2 - absorbed on the mirror                      21459
 -1 - did not make it out the agel                 1378
  0 -                                                 0
  1 - blocked by agel exit mask                    191
  2 - ray fell outside the flat mirror active area 1162
  3 - ray fell outside 1st lens diameter            499
  4 - ray fell outside Kaon hole                   1368
  5 - ray fell outside 2cd lens diameter              0
  6 - ray came backwards out of the light guide     172
  7 - ray reached the PMT face                      247
```

item	'93 test	Pb 94	fraction of last step (%)	MC mean 1K p.e.
'93 beam test				8.64
aerogel n	1.030	1.021	67	5.82
aerogel clarity C	183	185	99	5.75
aerogel surface A	0.96	1.00	104	5.98
aerogel thickness	3 cm	8.1 cm	176	10.52
particle velocity	1.00	0.002	58	6.16
track spread	no	yes	102	6.28
ring mask	6.5 cm	2.25	78	4.91
PMT efficiency	25%	25%	100	4.91
mirror reflectivity	92%	84%	94	4.64
fresnel losses	no	yes	99	4.62
backward fresnel	no	yes	96	4.45
second lens	no	yes	79	3.53
light cone	no	yes	81	2.87
optimized geometry	yes	no	64	1.85

Table 3: Monte Carlo calculation starting with '93 beam test configuration and going to Pb '94 configuration one effect at a time.

```
Total:    88423   88423
Mean # bounces in the light guide:  1.4+-   .6
At tube with 90%eff:     212.
          per event:       2.
```

Notice that the Monte Carlo keeps track of where the photons are lost and by what mechanism. From this information, we can make adjustments and modifications to the detector to improve on the number of photoelectrons seen per kaon.

A set of runs was done to see how we got from the observed 8.64 photons in the 1993 tests to the 2.0 or so seen in the 1994 lead beam runs. The MC was set up to represent the 93 conditions, removing items and effect that were not present. Then elements were added or exchanged, and the final configuration corresponds to what was in the beam in '94. The results are summarized in table xxx:

11 Retrospective

The succesful beam tests with the small fixture that were done in 1993 [7] showed 9 photoelectrons in the cherenkov ring. A decision needed to be made whether or not to go ahead and build a trigger counter, and what kind of device this should be - a differential counter or a spot imager. At the time, there was no full MC, so we scaled by known factors. These factors are summarized in the top half of table II, in the column labeled 'projected'. In the column labeled 'Pb 94' are the values for the items that we actually had in place for the '94 lead run.

It was argued that all other crucial elements were already present in the test ficture:

item	'93 test	projected	effect(%)
aerogel n	1.030	1.020	−50
aerogelgel clarity/thickness	200/3cm	100/8cm	+48
particle velocity	1.00	0.992	−25
PMT efficiency	25%	30%	+20
	9 p.e		7 p.e.

Table 4: Table II: scaling factors between the 1993 beam test fixture, and the projected trigger counter.

the acrylic lens, and the mirror (curved in the test, flat in the trigger counter). Liouville's theorem argued that it would be possible to map the kaon ring onto a 1.5" diameter tube without loss, by conservation of geometrical area.

12 Proposed modifications

Before we can try to make improvements on the detector design, we need some standard by which the results can be compared. For this purpose, we refer back to the section discussing the trigger. From the Monte Carlo ntuple, we can plot the two-kaon efficiency and the cleanliness as a function of photomultiplier ADC threshold for the trigger. We then require the number of triggers presented such that the live time maximizes the number of kaon pairs actually written to tape. We take the maximum rate to tape as 600 per burst (taken from tape log when triggers presented was 1M). Then, triggers accepted is calculated by equation 5.

A 1% target (0.5mm Pb) and a beam rate of 5M/burst, gives 50,000 events per burst. With RQMD multiplicities, 185 of these events are two or more kaon events. If we had a perfect two-kaon trigger, with equation 5 we could only accept 141 or 76% of them. With half of the beam rate, we would have 93 two-kaon events, and accept 80 of them or 86%. We will assume the 5M/burst beam rate (185 two-or-more-kaon events per burst), and adjust the trigger to maximize the number of two-kaon events written to tape. We can then also analyze the two-kaon events not accepted (from being excluded by the trigger, not the tape rate) to see if we introduce a bias in the data.

case	improvement	1K pe	fraction	efficiency	cost
1	Pb94	1.90	16%	20%	$0.
2	geometry	3.27	19%	26%	$0.
3	aerogel*	4.66	21%	32%	$14,500.
4	mirror	5.12	32%	35%	$500.
5	large PMT	7.04	32%	40%	??
6	case 5 - agel	4.43	19%	31%	
7	mult. APDs	21.2	74%	62%	$50,000.

Table 5: Monte Carlo results for different improvements. See text for details.

Table 5 lists this figure of merit for several improvements proposed for the cerenkov

detector. Each case will be described in detail below.

Case 1 This is the "base-line" case and is the exact situation which we had for the 1994 Pb beam run, except that we assume that the aerogel covers the whole acceptance with no seams. In that regard, the cost is inaccurate. However, if we replaced the aerogel (which we have to do in any case), we would get higher quality aerogel. This is intended only as a reference, not a possible option.

Case 2 Same situation as case 1, except the geometry has been optimized. This only requires a brief opening of the detector and a realignment. This includes putting the 1st fresnel lens in properly, which should be done in any case, and replacing the 2cd fresnel lens.

Case 3 This has the new aerogel as ordered from Lockheed. Index of refraction is 1.021, AHUNT = 1.000, CHUNT = 0.0100. Thickness is 9cm and it covers the whole acceptance. The cost of this aerogel was included in the original estimate for the detector.

Case 4 This case has the optimized geometry, new aerogel, and a new thin mirror with reflectivity of 90% throughout the wavelength region of interest.

Case 5 This is the same as case 4 but with a large diameter PMT (eight inch diameter) with efficiency which peaks at 25%. In this configuration, the second fresnel lens and the light guide are no longer in the geometry.

Case 6 This is the same as case 5 except the aerogel has a clarity (chunt value) of 0.0185. We have seen this clarity in almost all aerogel we have purchased.

Case 7 Same as case 5, except approximately fourty avalanche photodiodes are used instead of a phototube. This option is costly because of the price of avalanche photodiodes, and the development of the needed quenching electronics, and is only presented as a possible future improvement.

As a reference to what we can do without this detector, during the lead run kaon pairs running (run 3357 - rejecting pions with the jaws at 6 GeV), we used a beam rate of 2.48M/burst and had 295 triggers presented with 194 accepted. After analysis, only 0.2% of the events on tape were true kaon pairs. So, if the beam were 5M/burst, one would have 600 triggers presented with 300 accepted and only 0.65 real two-kaon events written per burst. Compare with case 6 where we accept 76 real kaon pairs per burst. We can collect statistics 115 times faster and with a cleaner sample on tape.

13 Conclusions

Since the lead runs, the data analysis, bench tests of components, and Monte Carlo investigations have led to a better understanding of the Aerogel trigger counter. Several relatively minor corrections to the device are expected to lead to much improved performance. These are: (1) small adjustments to the positions of the aerogel and the lenses, and (2) flipping over the big lens. Further gains can be made by (3) obtaining aerogel from Lockheed with quality as negociated in the contract, and (4) replacing the small PMT with a bigger tube, and eliminating the collection cone and second lens in the process.

14 Appendix I - Aerogel Manufacturers

Airglass, box 150, s-245 00 Staffanstorp, Sweden. phone (46) 46-25 60 83, fax (46) 46-25 69 20. Sten Henning is the person we talk to.
Airglass is the traditional supplier to the High-Energy community. They use the old one-step process. One of the consequences of this is that they can produce only a very limited range of refractive indices, and seem not to have good control of this crucial parameter. One order for n=1.020 came in at n=1.026. The quality of their products has been decidedly mixed. Surfaces are not particularly clean and flat. As for clarity, the best sample we've seen had Chunt=150, the worst Chunt=240 (xxx check these values).

At Livermore: Craig West, Larry Hrubesh, Chemistry, Materials Science, Lawrence Livemore Laboratory, Livermore, CA 94550. Phone (510) 423 1691. This group has made some good aerogel, and he has worked some with the SLAC b-factory people on trying to dope the a'gel with wavelength shifter, for readout with a fiber to an APD (avalanch photodiode.) I have not seen any results, but I think this doping was not a success. I believe he uses the two-step method.

Lockheed: David Mendez, Orgn 91-10 bldg 255, 3251 Hanover St. Palo Alto, Ca. Contact person is Jim Ryder (415) 424 2171. After years of delay, they resumed production in December 1995. They seem to have the best process control in the industry, so much so that they will guarantee in a contract to deliver material with Chunt=100+-10. Their own use for the material is for the capture of hyperverlocity particles in space.

Jet Propulsion Lab, Pasadena, Ca. Contact person is Peter Tsou, phone (818) 354 8094. Peter makes good aerogel, currently he produces at n=1.004. A sample of this came in at Chunt=95. He wants it also for catching space dust. He is working with James Oyang, who wants n=1.004 and n=1.020 for the Slac b-factory. He has made 10x10x10 recently at the lower density. We got blocks in 1994 with n=1.021, Chunt=185. The surfaces of this material was superior (compared to Airglass). The fact that Chunt came out high at n=1.020 is an indication that he needs a better understanding of the process to optimize this parameter.

15 Appendix II - Optimizing the light collector.

(include existing writeup)

References

[1] Richard C. Fernow, Introduction to experimental particle physics. Cambridge University Press (1986).

[2] P.A. Clausing, Inc. 8038 Monticello Ave., Skokie, IL 60076-3438.

[3] Fresnel lenses were purchased from Fresnel Optics, Inc. 1300 Mt. Read Blvd. Rochester, NY.

[4] Edmund Scientific Company, 101 E. Gloucester Pike, Barrington, NJ 08007-1380.

[5] M. Cantin et al., Nucl. Inst. Meth. **118** (1974) 177, M. Bourdinot et al., Nucl. Inst. Meth. **136** (1976) 99, M. Benot et al., Nucl. Inst. Meth. **154** (1978) 253, C. Arnault et al., Nucl. Inst. Meth. **177** (1980) 337, P.J. Carlson et al., Nucl. Inst. Meth. **192** (1982) 209, K. Maurer et al., Nucl. Inst. Meth. **224** (1984) 110, C. Fernandez et al., Nucl. Inst. Meth. **225** (1984) 313, H. Kawai et al., Nucl. Inst. Meth. **228** (1985) 314, P. Carlson, Nucl. Inst. Meth. **A248** (1986) 110, G. Poelz, Nucl. Inst. Meth. **A248** (1986) 118, P. Vincent et al., Nucl. Inst. Meth. **A272** (1988) 660, A. Onuchin et al. Nucl. Inst. Meth. **A315** (1992) 517, C. Lippert et al., Nucl. Inst. Meth. **A333** (1993) 413, T. Hasegawa et al., Nucl. Inst. Meth. **A342** (1994) 383.

[6] H. van Hecke, D.E. Fields, J. Boissevain, B.V. Jacak, W.E. Sondheim, J.P. Sullivan, W.J. Willis, P.M. Peters; A spot imaging Cherenkov counter. Nucl. Inst. Meth. **A346**, 127 (1994).

[7] D.E. Fields, H. van Hecke, J. Boissevain, B.V. Jacak, W.E. Sondheim, J.P. Sullivan, W.J. Willis, K. Wolf, E. Noteboom, P.M. Peters, R. Burke; Use of aerogel for imaging Cherenkov counters. NIM **A349**, 431 (1994).

[8] H. Beker et al., Phys. Lett. **B302** (1993) 510.

[9] The sample has a refractive index of 1.030, and was produced by Airglass Inc., Box 150, S-245 00 Staffanstorp, Sweden.

[10] Thorne EMI Electron Tubes Limited, Bury Street Ruislip Middlesex HA4 7TA England.

[11] A. Beck et al., 2cd International Symposium on Aerogels, ISA2 Montpellier, France, Sep. 21-23, 1988. Ed. R. Vacher, Les Ulis, France, Editions de Physique (1989).

[12] RCA Photomultiplier Handbook, RCA Electronic Components, Harrison, N.J. (1970).

[13] D. Mendez, Lockheed Research and Development 3251 Hanover Street Palo Alto, CA 94304; L. Hrubesh, Chemistry and Materials Science Lawrence Livermore Laboratory, Livermore, CA 94550; P. Tsou, Jet Propulsion Laboratory, Pasadena, CA 91125; A. Hunt, Div. Energy Environment, Lawrence Berkley Laboratory, Berkley, CA 94720.